Materials and Design 183 (2019) 108085

Contents lists available at ScienceDirect

Materials and Design

journal homepage: www.elsevier.com/locate/matdes

Effective design space exploration of gradient nanostructured materials using active learning based surrogate models

Xin Chen [a], Haofei Zhou [b,*], Yumeng Li [a,*]

[a] Department of Industrial and Enterprise Systems Engineering, University of Illinois at Urbana-Champaign, Urbana, IL 61801, United States
[b] Department of Engineering Mechanics, Zhejiang University, Hangzhou, Zhejiang, PR China

HIGHLIGHTS

- An efficient adaptive material design platform is established for accelerating novel material discovery and design.
- Potential of adaptive sampling is demonstrated in balancing the trade-off between fidelity and efficiency in material design.
- The collective effects of grain and twin gradients on strength and deformation mechanisms of GNT metals is uncovered.
- The importance of creating sufficiently large twin gradients in realizing the full potential of GNT metals is demonstrated.

GRAPHICAL ABSTRACT

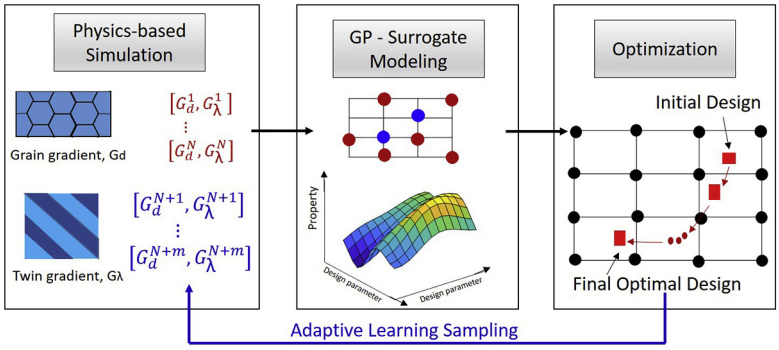

ARTICLE INFO

Article history:
Received 8 April 2019
Received in revised form
30 June 2019
Accepted 29 July 2019
Available online 2 August 2019

Keywords:
Materials design
Gradient nanostructured metals
Gaussian processes
Surrogate modeling
Artificial intelligence

Data availability:
The raw data required to reproduce these findings are available to download from Mendeley Data. The processed data required to reproduce these findings are available to download from Mendeley Data.

ABSTRACT

Inspired by gradient structures in the nature, Gradient Nanostructured (GNS) metals have emerged as a new class of materials with tunable microstructures. GNS metals can exhibit unique combinations of material properties in terms of ultrahigh strength, good tensile ductility and enhanced strain hardening, superior fatigue and wear resistance. However, it is still challenging to fully understand the fundamental gradient structure-property relationship, which hinders the rational design of GNS metals with optimized target properties. In this paper, we developed an adaptive design framework based on surrogate modeling to investigate how the grain size gradient and twin thickness gradient affect the strength of GNS metals. The Gaussian Process (GP) based surrogate modeling technique with adaptive sequential sampling is employed to develop the surrogate models for the gradient structure-property relationship. The proposed adaptive design integrates physics-based simulation, surrogate modeling, uncertainty quantification and optimization, which can efficiently explore the design space and identify the optimized design of GNS metals with maximum strength using limited sampling data generated from high fidelity but computational expensive physics-based simulations.

1. Introduction

Recently, gradient nanostructured (GNS) metals, including gradient nanograined (GNG) metals and gradient nanotwinned

* Corresponding authors.
E-mail addresses: xinc4@illinois.edu (X. Chen), haofei_zhou@zju.edu.cn (H. Zhou), yumengl@illinois.edu (Y. Li).

https://doi.org/10.1016/j.matdes.2019.108085

(GNT) metals, have emerged as a new class of materials with tunable microstructures. GNS metals could be designed to exhibit an unusual combination of ultrahigh strength, good tensile ductility, enhanced strain hardening, superior fatigue and wear resistance [1–5]. Using surface mechanical grinding treatment (SMGT), Fang et al. [1] prepared a GNG Cu specimen with a doubled yield strength and a comparable ductility with respect to coarse grained Cu. In GNG interstitial free (IF) steel attained through surface mechanical attrition treatment (SMAT), Wu et al. [2] reported an extra work hardening behavior controlled by a unique combination of non-uniform deformation and multiaxial stresses. In a twinned induced plasticity (TWIP) steel, pre-torsion and subsequent tension can be applied to form a hierarchical nanotwinned structure with a gradient nanotwin density along the radial direction, leading to enhanced strength and ductility [3]. Recently, Cheng et al. [4] used a direct-current electro-deposition method to synthesize GNT Cu samples with combined gradients in grain size and twin thickness. Due to a unique patterning of geometrically necessary dislocations in grain interiors, a sufficiently large structural gradient led to an improved strength and work hardening that can exceed even the strongest component of the gradient microstructure.

Although GNS metals are shown to possess superior mechanical properties as compared with their gradient-free counterparts, it remains largely unknown whether there exists a specific gradient structure that optimizes their mechanical properties [6]. Existing manufacturing approaches, including surface tooling [7,8] and mechanical treatments [3,9], generate limited volume fractions of gradient surface layers or negligible degrees of structural gradient along the gradient direction. In addition, most previous studies were focused on only one type of gradient structure, which limits our ability to realize the full potential of GNS metals considering the collective effects of various gradient structures. For instance, a typical GNG structure synthesized by surface mechanical treatment possesses a gradient nanograined surface layer and a coarse-grained core. The grain size of the top-most surface layer usually ranges from dozens of nanometers to submicrons, while it increases to microns in the coarse-grained core [1,2]. Recently, Lin et al. [10] used electrodeposition to prepare GNS Ni samples with a similar change in grain size from 29 nm to 4 μm. The degree of size gradient could be accurately controlled. It is observed that a maximum uniform elongation that exceeds even that of coarse-grained Ni could be achieved at an optimal profile of gradient size distribution, indicating that the ductility of GNS metals can be optimized through control of structural gradient. Although tremendous efforts have been spent in recent years to understand the underlying mechanisms that potentially lead to improved performances of the GNS materials, the challenges remain in fundamentally understanding the gradient structural-property relationships for optimizing the GNS metals for desired performances, which in turn largely hinders optimized designs and potential broad applications of GNS metals.

To address these challenges, the atomistic simulations, which have demonstrated their successes in the study of material systems such as nanocomposites [11–16], have been employed by researches to help discover potential mechanistic principles governing the behavior of GNS metals [17–19], considering the length scale of the gradient structures. Large-scale molecular dynamics (MD) simulations have been performed by Li et al. [17] to investigate the tensile properties and the related atomistic deformation mechanisms of the gradient nanograined (GNG) structures in bcc Fe. In this paper, comparison has been done for bcc Fe with gradient and uniform nanograined structures, which demonstrates that the gradient structure results in extra hardening and therefore higher flow stress. The dominating deformation mechanisms have been found to be closely correlated with the grain size in the GNG structures. Kai et al. conducted MD simulations to investigate the plastic deformation of a GNG copper film [18]. Extra strengthening was observed in the GNG film compared with the rule-of-mixture, which is believed to result from the orderly plastic deformation process attributed to the GNG structure. For GNT metals, Cheng et al. employed the atomic simulations for the study of a new strengthening mechanism governed by the simultaneous activation of threading dislocations and Hall-Petch type dislocations [19]. In their study, the mechanism prevailed in a columnar-grained nanotwinned metal subject to an external stress parallel to the twin planes. A unique patterning of geometrical necessary dislocations was observed in the form of bundles of concentrated dislocations uniformly distributed in grain interiors, which is fundamentally different from randomly distributed, statistically stored dislocations in homogeneous structures. Although atomic simulation could often help reveal mechanisms that could potentially yield superior mechanical performances, it is still computationally prohibitive for purely relying on the atomic simulations to explore a multidimensional parameter space for optimizing the design of the materials.

On the other hand, in the engineering design community, to tackle the challenge in repeatedly evaluating expensive black-box functions in the design space during the design optimization process, advanced surrogate modeling techniques have been employed to improve the efficiency of design space exploration [20–24]. To further improve the efficiency and reduce the cost in conducting the design of experiment (DOE), advanced sampling techniques have been developed in the literature to adaptively choose useful sample points in the design space to be evaluated for sequentially improving the fidelity of surrogate models. A crucial issue in sequential surrogate modeling is the sampling strategy used to generate sample points in order to construct the initial low fidelity surrogate model. The one-step sampling method, i.e. Latin hypercube sampling (LHS) method [25,26] has been widely used for this purpose. By using the LHS, the random input domain will be occupied most evenly by sample points, thereby enabling much information about the true model to be obtained. However, it usually provides similar sample point profiles to occupy the random input domain evenly regardless of the distribution of true system responses. On the contrary, the importance sampling technique [27,28] generates sample points around the limit state area and predicts the response accurately around the limit state. However, it usually only provides good local surrogate models and does not represent the true model accurately enough in other areas of the random input domain. Besides the LHS method and the importance sampling method, there are other advanced sampling techniques, such as the Improved Distributed Hypercube Sampling (HIS) [29], orthogonal-array-based LHS designs [30], and maximin LHS designs [31], which can all be used to generate sample points to construct the initial surrogate model. A comparison of these different sampling methods can be accordingly found in the literature [32].

The goal of this work is to develop an effective material design space exploration framework that can help deepen the understanding of the following fundamental questions: how do structural gradients in grain size and twin thickness affect the strength and plastic deformation mechanisms of GNS metals? And does there exist a specific structural gradient that optimizes their strength? In this work, an adaptive design framework is developed to address the above mentioned challenges and answer those questions through the integration of MD simulations, simulation-based surrogate modeling, uncertainty quantification and optimization. Uniaxial tension simulations have been conducted using MD simulations to evaluate the strength of GNT Cu samples with various gradients in grain size and twin thickness. Therefore, the collective effects of grain and twin gradients can be investigated for their effects on strength and deformation mechanisms of GNT Cu. Gaussian process (GP) is adopted for constructing surrogate model based on physics-based simulations, which is MD simulations in our work, to predict the material property in the design region

without experimental and simulation sampling data. Surrogate modeling based machine learning techniques are emerging as powerful tools in material science and engineering [33–37] for revealing the underlying governing mechanisms and accelerating the material design. GP process used in our study is a non-parametric Bayesian machine learning technique, which returns robust variance estimates of predictions for uncertainty quantification without extra computational cost [22,38]. With adaptive sampling techniques, an iterative design loop is realized to explore the design space in an efficient manner with computational expensive physics-based simulation only performed in critical regions. GNT material system with the optimized strength is identified through the design iteration and validated through physics-based simulation. The present results are expected to shed lights on the design of GNS structures for optimal mechanical properties.

The remainder of the paper is organized as follows. In Section 2, the GNT Cu material system is introduced and the developed MD simulation model for GNT Cu is explained. In Section 3, the GP based active learning surrogate modeling technique is detailed and demonstrated with an analytical example. Two defined design parameters are described for characterizing the corresponding gradient structures in GNT Cu. Flow stress is calculated for GNT Cu models with various gradient nanostructures. The adaptive sampling strategies for gradually increasing the fidelity of the surrogate model based on uncertainty quantification are discussed. In Section 4, the GP active learning surrogate modeling technique is applied to the design space exploration of the GNT Cu material systems, and the results and insights from both MD simulation and adaptive design process are discussed. The established surrogate model is validated and the identified optimal design of GNT Cu with maximum flow stress is reported. The underlying deformation mechanisms in GNT Cu governing the established gradient structure-property relationship are discussed based on MD simulations results. Finally, Section 5 offers some conclusive remarks.

Nomenclature

β	GP regression coefficient
Corr	correlation function
d	grain size
λ	twin thickness
g_d	gradient of grain size
g_λ	gradient of twin thickness
$G_{GP}(\mathbf{x})$	Gaussian process predictor
$\hat{e}$ $(\mathbf{x})$	mean square error
R	correlation matrix
Ψ	the likelihood function

2. GNT copper and atomic simulations

This section introduces the GNT Cu as the material system for the presented materials design study, and also provides the information about Molecular Dynamic (MD) simulations that will be used as the physics-based computational methodology for generating high fidelity sample points in the design space to explore the effects of grain size and twin thickness gradients on the strength of GNT Cu.

2.1. The GNT Cu material system

With the decrease of the grain size, the strength of polycrystalline materials generally increases. On the other hand, smaller grains might lead to softening when the size is below a critical value. The strongest size should arise at a transition in deformation mechanism from lattice dislocation activities to grain boundary–related processes. Studies have been reported in the literature [39] that investigated the maximum strength of nanotwinned Cu samples with different twin thicknesses, and found that the strength increases with decreasing twin thickness and the strongest twin thickness originates from a transition in the yielding mechanism from the slip transfer across twin boundaries to the activity of pre-existing easy dislocation sources. Additionally, materials with structural gradients often have unique combinations of properties. A recent study [4] developed a structural gradient by introducing gradients of crystallographic twins into copper. The presented strategy would create bundles of dislocations in the crystal interiors, making the metal stronger than any of the individual components, which offers promise for developing high-performance metals.

In this study, GNT Cu is investigated for the material system design study, and specifically fully three-dimensional GNT Cu structures containing two homogeneous columnar-grained nanotwinned components with $[1\bar{1}1]$ out-of-plane texture (NT-A and NT-B) are considered, as shown in the Fig. 1. In order to quantify the gradients in grain size and twin thickness, two structural parameters, $g_d = d_B/d_A$ - 1 and $g_\lambda = \lambda_B/\lambda_A - 1$ have been defined, where grain size and twin thickness are denoted as d_A and λ_A in NT-A, and d_B and λ_B in NT-B, respectively. NT-A and NT-B have equivalent grain size and twin thickness when $g_d = 0$ and $g_\lambda = 0$.

2.2. Atomistic simulations of the GNT Cu

To consider effects of the grain size and twin thickness, the GNT Cu samples were constructed for atomistic simulations. Each GNT sample contains ~21,000,000 atoms and has dimensions of ~$100 \times 100 \times 25$ nm^3. The volume fractions of NT-A and NT-B are equal in each GNT sample. The structure of homogeneous component NT-B used to generate the GNT samples was fixed to possess

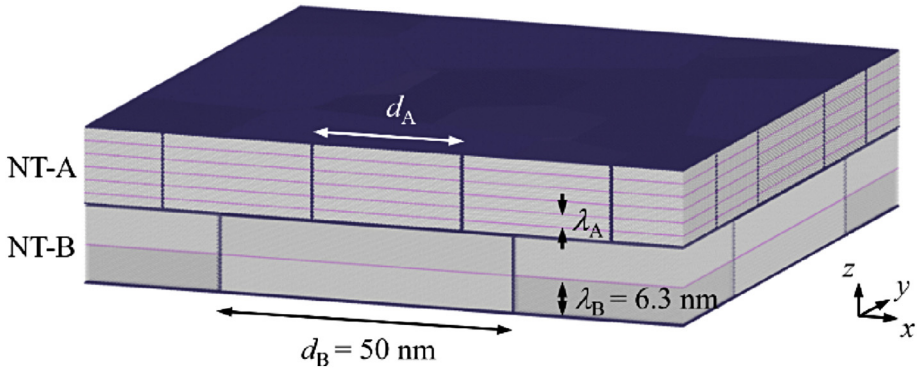

Fig. 1. A typical GNT sample in MD simulations composed of two homogeneous nanotwinned layers NT-A and NT-B forming grain size and twin thickness gradients along the z-axis. Grain size and twin thickness are denoted as d_A and λ_A in NT-A, and d_B and λ_B in NT-B. Uniaxial tensile loading is applied along the x-axis.

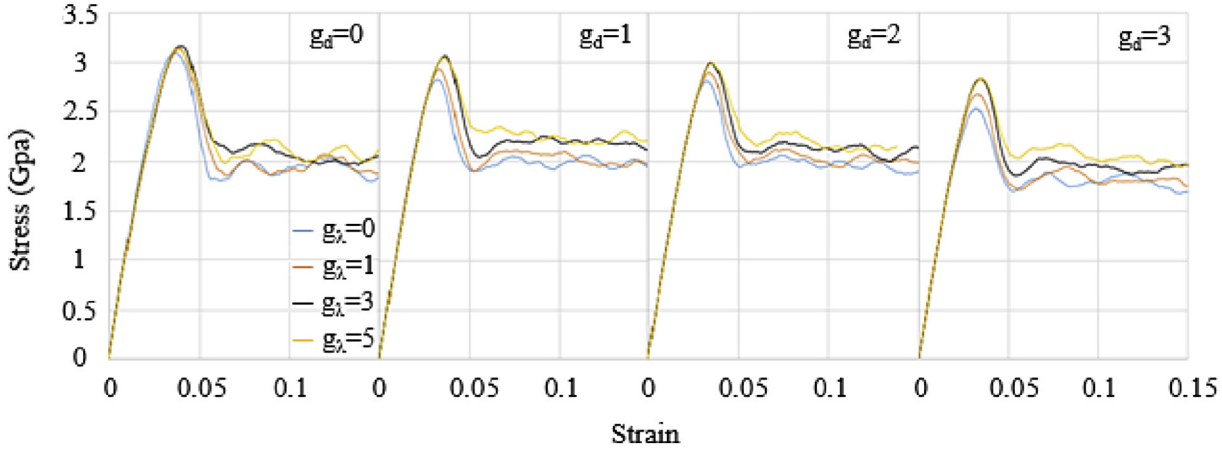

Fig. 2. Stress-strain relations and flow stress of the simulated GNT Cu samples. Stress-strain curves of GNT Cu with different values of grain and twin gradients, g_d and g_λ.

average grain size of $d_B = 50$ nm and twin thickness of $\lambda_B = 6.3$ nm. By varying the grain size (d_A) and twin thickness (λ_A) of the homogeneous component NT-A, GNT samples with various gradients in grain size and twin thickness were generated.

The system was initially equilibrated at 300 K for 500 ps, followed by uniaxial tensile loading along the x-axis to a total strain of 15% at a constant strain rate of $5 \times 10^8\ s^{-1}$. Throughout the simulation, periodic boundary conditions were applied in all three directions. Constant temperature and zero pressure in the non-stretching directions (i.e., y- and z-axes) were controlled by Nose-Hoover thermostatting and barostatting [40,41]. The embedded atom method potential [42] was used to compute the interatomic forces, and the integration time-step was fixed at 1 fs. The common neighbor analysis (CNA) method [43] was used to identify defects that emerge during plastic deformation. Strain-stress responses were monitored during the MD simulations for GNT Cu samples with various gradient structures to characterize their mechanical performance as shown in Fig. 2. The yield strength for each sample was calculated in terms of average flow stress over the strain range of 6 to 15%.

3. Active learning surrogate model

This section introduces the active learning surrogate modeling technique that will be employed together with the physics-based atomistic simulations for effective material design space exploration in order to identify optimized grain size and twin thickness on the strength of GNT Cu. Section 3.1 introduces the surrogate modeling technique based on the Gaussian process models; Section 3.2 explains the active learning using a confidence based sequential sampling method for efficient enhancement of the fidelity of surrogate models. Section 3.3 summarizes the procedures of using the active learning surrogate models for materials design space exploration, and Section 3.4 provides an analytical example for demonstrating the proposed method.

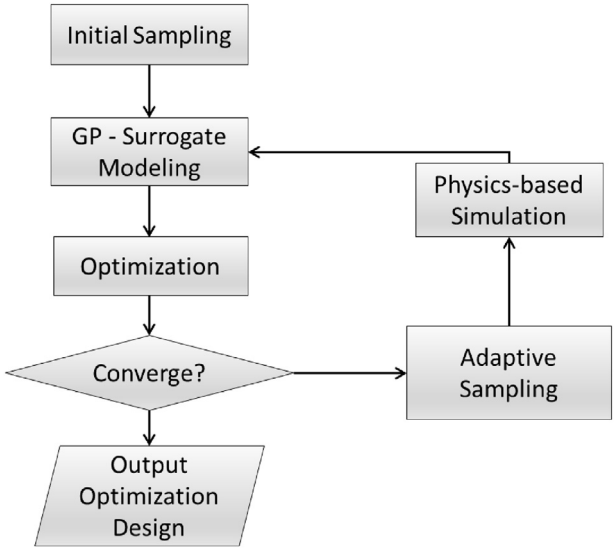

Fig. 3. The schematic adaptive design framework based on GP-Surrogate modeling.

3.1. Gaussian process based surrogate modeling

It is often extremely challenging and costly to dig into the optimization problem of GNS metals using experimental or physics-based computational methods, which is the MD simulation method in the present study. Indeed, our MD simulations have investigated limited design parameters featuring the structural gradients in grain size and twin thickness of GNT, which leaves vast unexplored design spaces. To address the challenges associated with the optimized design of GNT metals, we established an adaptive design framework schematically shown in Fig. 3, which integrates physics-based simulations, surrogate modeling, uncertainty quantification and optimization. The key components of the developed adaptive design framework include: 1) an initial sparse random training data set from MD simulations; 2) surrogate model that uses the training data set to learn the feature-property relationship; 3) uncertainty quantification of the surrogate model for updating; 4) identifying the critical new sampling points for updating the surrogate model to improve the fidelity; 5) the use of the converged surrogate model to search the unexplored design space for optimized design.

In this study, a Gaussian Process (GP) based surrogate model is employed to establish how the strength of GNT metals varies with the input features $\mathbf{x}$ over the whole chosen design domain. While using the GP regression, the material performance is assumed to be generated as

$$G(\mathbf{x}) \approx G_{GP}(\mathbf{x}) = \mathbf{f}^{\mathbf{T}}(\mathbf{x}) \cdot \beta + S(\mathbf{x}) + \varepsilon \quad (1)$$

where $\mathbf{f}^{\mathrm{T}}(\mathbf{x}) = [f_1(\mathbf{x}), \ldots, f_b(\mathbf{x})]$ is the base functions, $\boldsymbol{\beta} = [\beta_1, \beta_2 \ldots, \beta_b]$ the regression coefficient vector, S($\mathbf{x}$) the Gaussian stochastic process with zero mean and certain covariance matrix, and ε the uncorrelated noise that follows normal distribution. Generally, $\mathbf{f}^{\mathbf{T}}(\mathbf{x})\ \beta$ can be replaced by a constant global mean μ based on the fact that a constant mean in GP model is generally adequate to model the performance function. By assuming noise-free observations, the GP model can be written as:

$$G_{GP}(\mathbf{x}) = \mu + S(\mathbf{x}) \tag{2}$$

In the GP model shown in Eq. (2), the Gaussian covariance function is adopted for the stochastic process S(x). For two random inputs x_i and x_j, the Gaussian covariance function can be expressed as

$$\mathbf{Cov}_{(i,j)} = \sigma^2 \mathbf{R}_{(i,j)} \tag{3}$$

where **R** is the correlation matrix. The (i, j) entry of the matrix **R** is described as

$$\mathbf{R}_{(i,j)} = Corr(\mathbf{x}_i, \mathbf{x}_j) = exp\left[-\sum_{p=1}^{N} a_p \left| x_p^i - x_p^j \right|^{b_p} \right] \tag{4}$$

where Corr is the correlation function. a_p and b_p are parameters of the GP model. With n number of observations (X, Y) in which $X = [x_1, \ldots, x_n]$ and $Y = [y(x_1), \ldots, y(x_n)]$, the log likelihood function of the GP model can be given as

$$\Psi = -\frac{1}{2}\left[nln(2\pi) + nln\sigma^2 + ln|\mathbf{R}| + \frac{1}{2\sigma^2}(\mathbf{Y} - \mathbf{A}\mu)^T \mathbf{R}^{-1}(\mathbf{Y} - \mathbf{A}\mu) \right] \tag{5}$$

where **A** is an $n \times 1$ unit vector. Then μ and σ^2 can be obtained by maximizing the likelihood function as

$$\mu = \left[\mathbf{A}^T \mathbf{R}^{-1} \mathbf{A} \right]^{-1} \mathbf{A}^T \mathbf{R}^{-1} \mathbf{Y} \tag{6}$$

$$\sigma^2 = \frac{(\mathbf{Y} - \mathbf{A}\mu)^T \mathbf{R}^{-1}(\mathbf{Y} - \mathbf{A}\mu)}{n} \tag{7}$$

With the GP regression model, the response for any given sample point **x** can be estimated as

$$G_{GP}(\mathbf{x}) = \mu + \mathbf{r}^T \mathbf{R}^{-1}(\mathbf{Y} - \mathbf{A}\mu) \tag{8}$$

where r is the correlation vector between x and the samples $X = [x_1, \ldots, x_n]$, and the i-th element of r is given by $r(i) = Corr(x, x_i)$. The mean square error $\hat{e}(x)$ can be accordingly estimated by

$$\hat{e}(\mathbf{x}') = \sigma^2 \left[1 - \mathbf{r}^T \mathbf{R}^{-1} \mathbf{r} + \frac{\left(1 - \mathbf{A}^T \mathbf{R}^{-1} \mathbf{r}\right)^2}{\mathbf{A}^T \mathbf{R}^{-1} \mathbf{A}} \right] \tag{9}$$

It is noted that employing a GP-based surrogate model allows the uncertainty quantification of the prediction over the whole design domain through the estimated mean square error in a natural way.

3.2. Active learning using expected improvement-based sequential sampling

As the physics-based MD simulations are computationally expensive, we start with a low fidelity GP-based surrogate model based on a small size of initial random sampling $[X_E, Y_E]$. Then the GP-based surrogate model will be updated with new sampling points to enhance the fidelity gradually. Therefore, an active learning scheme is employed to determine the most wanted new sampling points for the sequential updating of the GP-based surrogate model. Various adaptive sampling approaches have been developed for surrogate model based engineering design problems to mitigate the cost of generating sampling points as well as to ensure the fidelity of the developed surrogate model. Liu et al. provided a good review of adaptive sampling techniques in support of simulation-based complex engineering design [44]. In our current study, the expected improvement-based sequential sampling scheme will identify the new sampling point to be where the highest uncertainty (i.e. the highest estimated variance) is observed or where the current possible maximum property is, in order to decrease the overall error of the GP-based surrogate model. True response value Y* of the selected new sample data X* will be calculated using MD simulations. Then [X*, Y*] is added to $[X_E, Y_E]$ and the GP-based surrogate model will be updated accordingly. GP-based surrogate model is updated iteratively by adding new sampling points until the overall error is below a certain threshold. After that, the GP-based surrogate model is used for providing the prediction of material property over the whole design space and identifying the optimized design by combing with optimization.

Table 1
The procedure of active learning for material design space exploration.

Steps	Procedure
Step 1:	Identify a set of initial samples, X_E, and evaluate the response of the material properties, Y_E, using atomic simulations;
Step 2:	Develop a GP model for $Y(X)$ with existing sample points, determine the global optimum approximation, Y_m, and the corresponding sample point, X_m;
Step 3:	At the ith sample iteration, determine the new sample point X_i with a maximum expected improvement $max\ \{E(I(X_i))\}$;
Step 4:	Compare max $\{E(I(X_i))\}$ with I_c: If max $\{E(I(X_i))\} \le I_c$, STOP and Report X_m and Y_m; Else, Go to Step 5;
Step 5:	Evaluate the response at X_i, and repeat Step 2 to Step 4.

This subsection introduces an active learning approach using expected improvement based sequential sampling (EISS) method for the sequential updating of the GP-based surrogate models. After developing the initial GP model, the active learning method updates this model iteratively through continuously searching the most useful sample point that ensures a maximum improvement for the accuracy until the convergence criteria is satisfied. To update the stochastic process model, the EISS method employs an expected improvement [23,24] metric to quantify the potential contribution of a new sample point to the existing response surface and the sample point that gives the largest expected improvement value will be chosen at next iteration. In what follows, the expected improvement metric will be introduced briefly.

Considering a continuous function $Y(x)$ over x, here we employ expected improvement metric to determine its global minimum. Based on a set of initial samples, $[X_E, Y_E]$, an initial GP model of $y(x)$ can be constructed and used to find out an approximation of the global minimum. However, due to limited samples, the initial model may introduce large model uncertainties and consequently

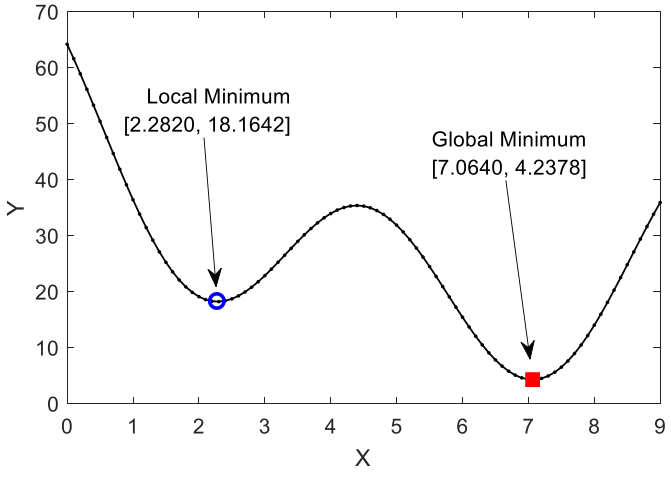

Fig. 4. Realization of the mathematic example.

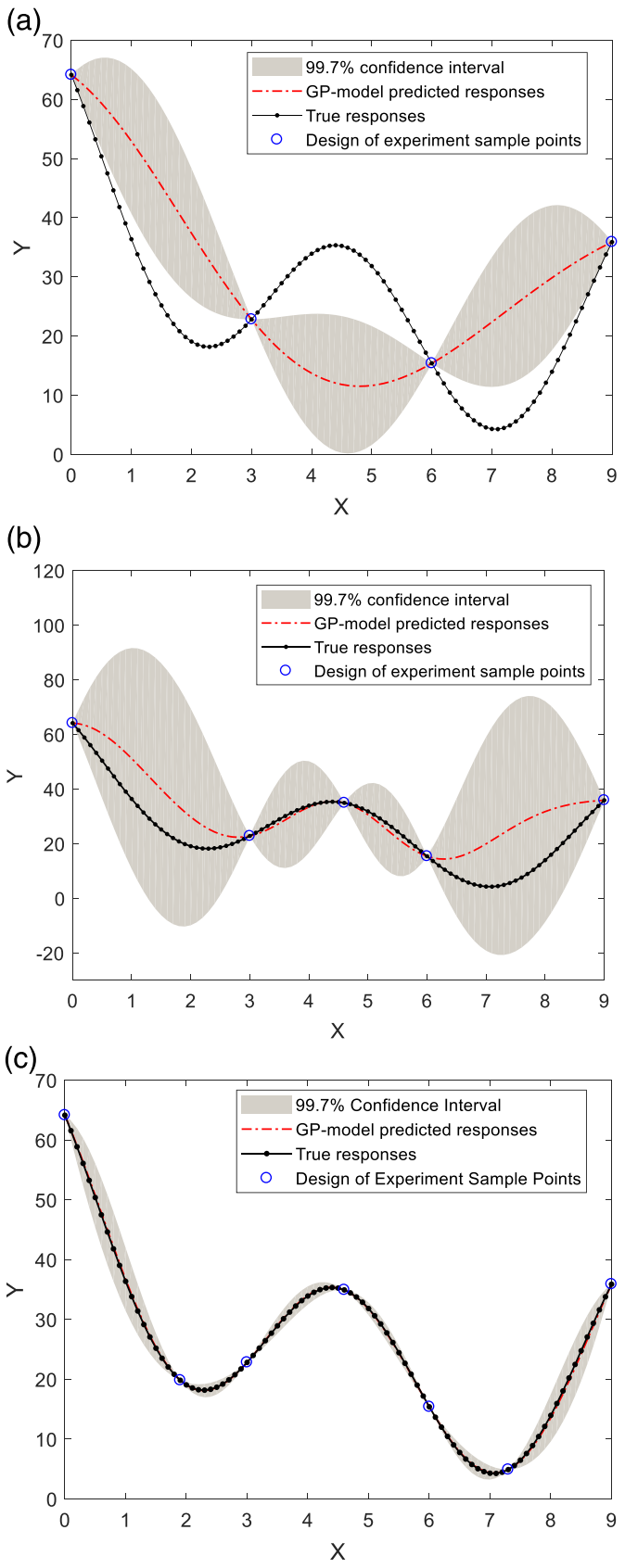

Fig. 5. (a): The initial low fidelity GP model with four sample points.
(b): The first active learning iteration for the adaptive surrogate modeling.
(c): The fourth active learning iteration for the adaptive surrogate modeling.

Table 2
The iterative process for global minimum identification.

Iteration	New sample point, t			Approximated global minimum	
	Max $E(I(x))$	x	$y(x)$	x_m	y_{min}
0	–	–	–	4.8031	11.5082
1	5.7997	4.5622	35.0641	6.2693	14.4075
2	87.6002	7.4928	6.3880	7.0248	3.4876
3	58.1245	1.4927	25.3070	7.0709	4.3672
4	0.2009	7.0269	4.2541	7.0620	4.2398

the function approximation, $y(x)$, could be substantially biased compared with the real function $Y(x)$. Due to the uncertainty involved in this model, the function approximation of $y(x)$ at x is treated as a Gaussian random variable whose mean and standard deviation are computed by approximated response, $Y_r(x)$ and its standard error, $e(x)$ from the GP model. With these notations, the improvement by sampling at x can be defined as

$$I(x) = max(Y_{\min} - y(x), 0) \tag{10}$$

where $Y_{\min}$ indicates approximated global minimum value at the current sampling iteration. By integrating the expectation of right part of Eq. (10), the expected improvement at any given sample point, x, can be presented as

$$E[I(x)] = E[max(Y_{\min} - y, 0)] = \left(F_{min} - Y_r(x)\right)\Phi\left(\frac{Y_{min} - Y_r(x)}{e(x)}\right) + e(x)\phi\left(\frac{Y_{min} - Y_r(x)}{e(x)}\right) \tag{11}$$

where $\Phi(.)$ and $\phi(.)$ are the cumulative distribution function and the probability density function for the standard Gaussian distribution respectively. As larger expected improvement at X means that the probability of achieving a better global minimum approximation is higher, thus a new sample should be evaluated at the particular sample point X* where the maximum expected improvement value is obtained to update the GP model. With the updated model, a new global minimum approximation for the $Y(x)$ can be obtained. The same process can be repeated iteratively through evaluating new sample point that provides the maximum expected improvement value and updating the GP model for new global minimum approximation, until the maximum expected improvement is small enough and less than a critical value I_c (in this study, $I_c = |F_{min}|\%$, which is 1% of the absolute value of the current best global minimum approximation).

3.3. Procedure of using active learning surrogate models

The procedure of employing the active learning surrogate modeling technique for efficient material design space exploration can be summarized as the following five steps as listed in Table 1, together with a flowchart as shown in Fig. 3.

3.4. An analytical example with active learning surrogate model

In this subsection, a one-dimensional analytical example is employed to demonstrate the active learning surrogate modeling technique using the expected improvement based sequential sampling method for efficient design space exploration. Assume that the structure property relationship is characterized by a one-dimensional performance function provided by

$$y(x) = x^2 - 12x + 15sin(1.2x + 2.4) + 54 \tag{12}$$

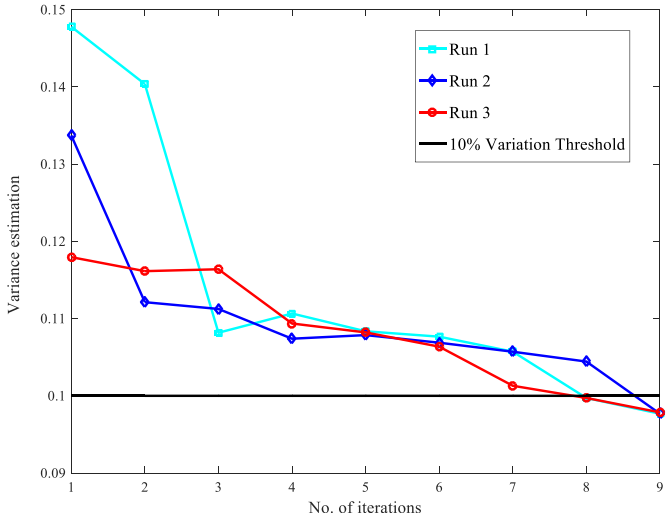

Fig. 6. The history of Maximum variance and uncertainty of the current optimization results over the design iteration.

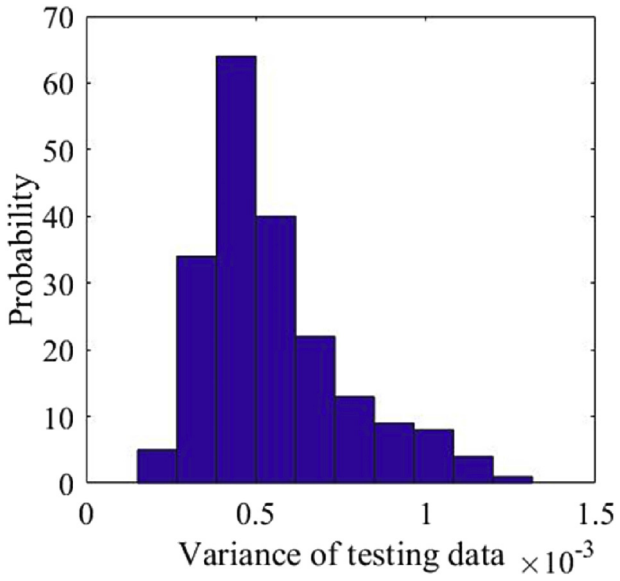

Fig. 7. The mean square error distribution for 5 folder cross validation analysis with 100 replicate runs.

The objective here is to identify the minimum response of $y(x)$ (the global minimum) and pinpoint the corresponding x within the design space [0, 9]. Fig. 4 shows the performance function, where the global minimum can be identified as $x = 7.0640$ with $y(7.0640) = 4.2378$, whereas the local minimum is located at $x = 2.2820$ with $y(2.2820) = 18.1642$.

Follow the procedures outlined in Table 1, the performance function is first evaluated at initial samples $x_1 \sim x_4$: [0, 3, 6, 9] and the obtained limit state function values are $y(x_1) \sim y(x_4)$: [64.1319, 22.8088, 15.3851, 35.8811]. With these initial sample points, a one-dimensional Gaussian process model can be built to approximate the performance function $y(x)$, as shown in Fig. 5a and the global optimum can be approximated as $y(4.8031) = 11.5082$. As the active learning surrogate modeling procedures summarized in Table 1, the expected improvement is calculated based on Eq. (11) throughout the interval [0, 9] and the maximum expected improvement can be obtained as $max\ \{E(I(t_i))\} = 11.3592$ where $x_1 = 4.6051$. Thus, the performance function will be evaluated at the new sample point $x_1 = 4.6051$ which results in $y(4.6051) = 34.9067$. Fig. 5b shows the above discussed the first active learning iteration for the global minimum response identification. In next iteration, by adding a new sample point to those existing ones, a new stochastic process model with better accuracy can be built for the approximation of $y(x)$ over the design space and the identification of the global minimum response of the performance function (global minimum). The procedures shown in Table 1 can be repeated until the convergence criterion is satisfied and the global minimum response of the limit state function is identified with a desired accuracy level. Fig. 5c shows the final iteration for the extreme response identification in which clearly the expected improvement of including a new sample point for the response surface is small enough and the convergence criterion is satisfied. Table 2 details all the iterations for the active learning surrogate modeling of this analytical example.

4. Design space exploration of GNT Cu using active learning surrogate modeling

This section demonstrates the application of the developed adaptive simulation-based surrogate model for efficiently exploring the design space of GNT Cu, and further identifying the optimal structural gradients of GNT Cu with maximum flow stress through combined with optimization. Then some insights are provided regarding the underlying mechanisms governing the relationship between the structure gradients and material property by carefully reading the results of MD simulations.

4.1. Active learning surrogate modeling of GNT Cu

As shown in Fig. 6, starting with a small number of sampling data points, the GP-based surrogate model is initially set up with a relatively low fidelity for the design space as shown in Fig. 9. During the iteration process, new sampling points are added to update the surrogate model, which shows a decreasing error as shown in Fig. 6. Due to the difficulty of preparing simulation models with high resolution, new sampling points are generated to have a close distance to the desired sampling points determined by the adaptive sampling rules. Three design runs are performed to start with different initial sampling points. They all exhibits decreasing error during the iteration history with new sampling data added.

Table 3 shows the iterative process for the active learning

Table 3
The iterative active learning process material design space exploration.

Iter.	Run 1				Run 2				Run 3			
	Max(EI)	X		Ymax	Max(EI)	X		Ymax	Max(EI)	X		Ymax
1	3.28E-05	4.48	1.74	2.20	1.06E-05	3.36	1.14	2.21	3.23E-05	4.40	1.28	2.24
2	3.88E-05	4.32	1.32	2.25	1.00E-05	3.28	1.14	2.21	2.84E-05	4.24	1.24	2.23
3	5.04E-05	4.00	1.41	2.25	9.80E-06	3.60	1.11	2.21	2.84E-05	4.24	1.24	2.23
4	3.13E-05	4.56	1.29	2.24	2.40E-05	4.48	1.23	2.24	2.66E-05	4.40	1.24	2.24
5	2.85E-05	4.88	1.29	2.25	2.07E-05	4.96	1.23	2.26	1.98E-05	4.48	1.20	2.26
6	2.18E-05	4.64	1.23	2.26	1.62E-05	4.80	1.20	2.26	2.23E-05	4.72	1.24	2.27
7	2.03E-05	4.80	1.23	2.27	2.07E-05	4.96	1.23	2.27	2.32E-05	4.64	1.24	2.26
8	2.09E-05	4.72	1.23	2.26	1.23E-05	4.80	1.17	2.27	2.23E-05	4.72	1.24	2.26
9	2.02E-05	4.88	1.23	2.27	2.02E-05	4.88	1.23	2.27	1.60E-05	4.88	1.20	2.27

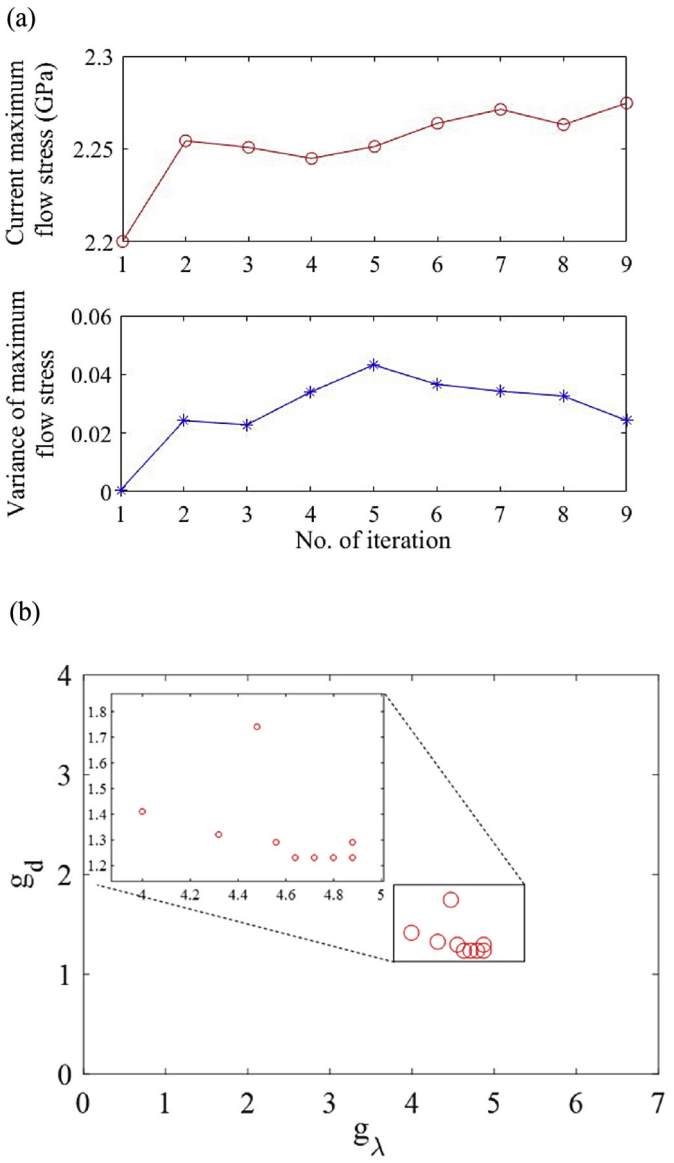

Fig. 8. The adaptive surrogate modeling and design optimization process: (a) the maximum flow stresses and corresponding prediction variances in each iteration, and (b) the predicted optimized design point in the 2D design space with maximum flow stress in each iteration.

surrogate modeling using expected improvement sequential sampling method (EISS), in which the maximum expected improvements at each iteration as well as the design parameters corresponding to the predicted maxim flow stress are shown. It can be observed that the expected improvement values are relatively small as the performance function values in this material design problem have been small as compared to the mathematical case study. To clearly show the convergence process for the active learn based sequential sampling method, the maximum prediction variances have also been recorded, and the values of the maximum variance have been reduced below 0.01 while more sample points are sequentially included. Optimization is complemented using the trained surrogate model with a desired fidelity. In all the iterations, a total of 20 sampling points are used. Five-fold cross validation analysis is conducted as shown in Fig. 7. It can be observed that the errors are centered around a low value, which demonstrates a good fidelity of the established surrogate model.

The optimized design is identified to be around $g_\lambda = 4.88$ and $g_d = 1.23$ with a prediction of maximum flow stress around

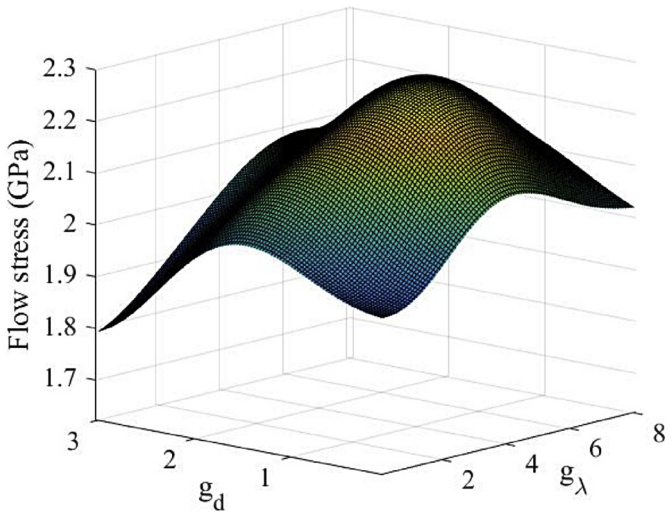

Fig. 9. Flow stress over the design space predicted by the GP-based surrogate model.

2.274 GPa. Due to difficulty of generating MD simulation model with high resolution, we conducted a simulation with $g_\lambda = 5$ and $g_d = 1$ close to the optimized design to validate our model. The simulated true flow stress is 2.256 GPa, while the predicted value is 2.265 GPa (error = 0.0039). This validates the optimized design and demonstrates the high fidelity of the established surrogate model. We plot the current maximum flow stress estimated in each step of one design iteration (top panel) and the corresponding variance (bottom panel) in Fig. 8a. Except for the first iteration, all the predicted maximum flow stresses stay in a small region between 2.245 and 2.274 GPa. We also plot the best design in each iteration in the design space (Fig. 8b). Most of the best designs are clustered in a small region. This demonstrates that, although a highly nonlinear relationship exists between the flow stress and the structural gradients (Fig. 9), high-fidelity surrogate model can still be established based on a limited size of sampling data.

4.2. Design space exploration results and insights from MD simulations

Tensile stress versus strain curves for GNT Gu samples with four different grain gradients g_d and four different twin gradients g_λ are shown in Fig. 10. It can be seen in Fig. 10a that, for a given g_λ, the average flow stress first increases with increasing g_d, reaching a maximum at $g_d = 1$, and then decreases with further increasing g_d. On the other hand, for a given g_d, the average flow stress increases monotonically with increasing g_λ (Fig. 10b).

To explain the gradient effect on average flow stress observed in Fig. 10, deformation patterns of the GNT samples with different structural gradients are examined (Fig. 11). The result for the layer NT-B in GNT samples with $d_B = 50$ nm and twin thickness of $\lambda_B = 6.3$ nm at 7.5% strain is shown in Fig. 11a where plastic deformation is governed by threading (mode II) dislocations. The movement of threading dislocations is confined inside the twin lamellae. Confined threading dislocations are frequently observed in highly oriented nanotwinned metals, nanoscale thin films and multilayered materials [45–47]. The stress required to move a threading dislocation can be expressed by the well-known confined layer slip (CLS) model in the form of [19]

$$\sigma_{CLS} = M\frac{\mu b sin\varphi}{8\pi\lambda}\left(\frac{4-\nu}{1-\nu}\right)ln\left(\frac{\alpha\lambda}{bsin\varphi}\right) + \sigma_0 \tag{13}$$

where μ is the shear modulus, ν the Poisson's ratio, M the Taylor factor, φ the angle between slip plane and the layer interface, b the

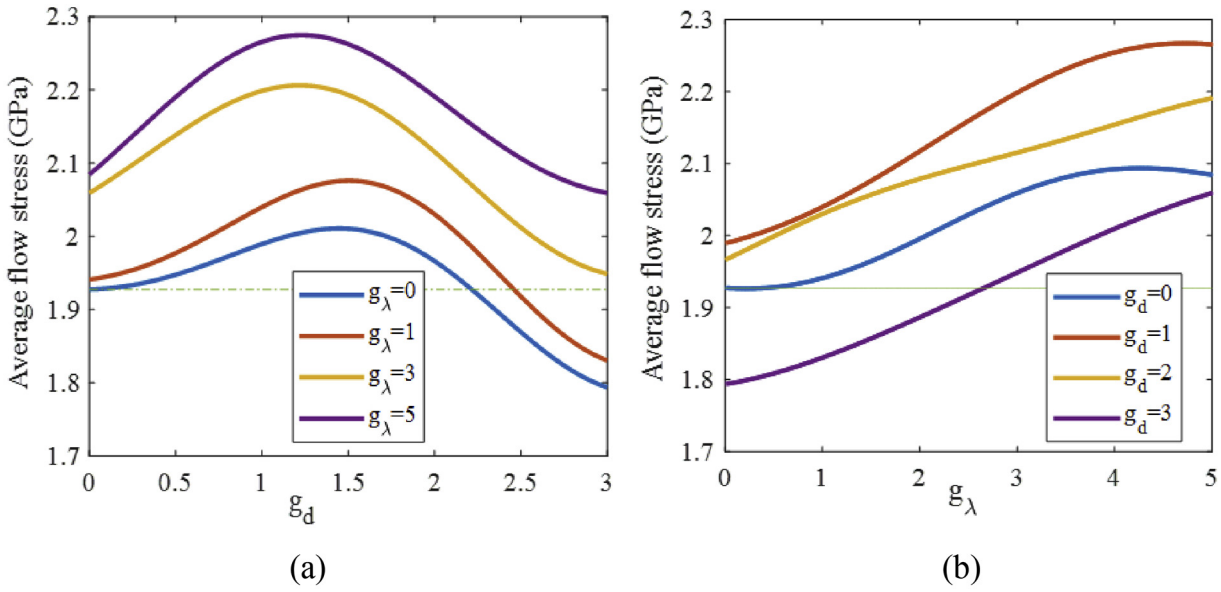

Fig. 10. Average flow stress as a function of g_d (a) and g_λ (b). The average flow stress is measured from a strain of 6–15% for all simulated samples as in Fig. 2.

Burgers vector of the dislocation and α a coefficient representing the extent of dislocation core. σ_0 represents the resistance to dislocation motion due to lattice friction, the prestress associated with the twin boundaries, and the interaction between the threading dislocation and a pre-existing array of misfit segments on the neighboring twin boundaries. Eq. (13) shows that the dependence of flow stress on twin thickness scales with $\lambda^{-1} \ln \lambda$. It leads to moderate strengthening when threading dislocations are

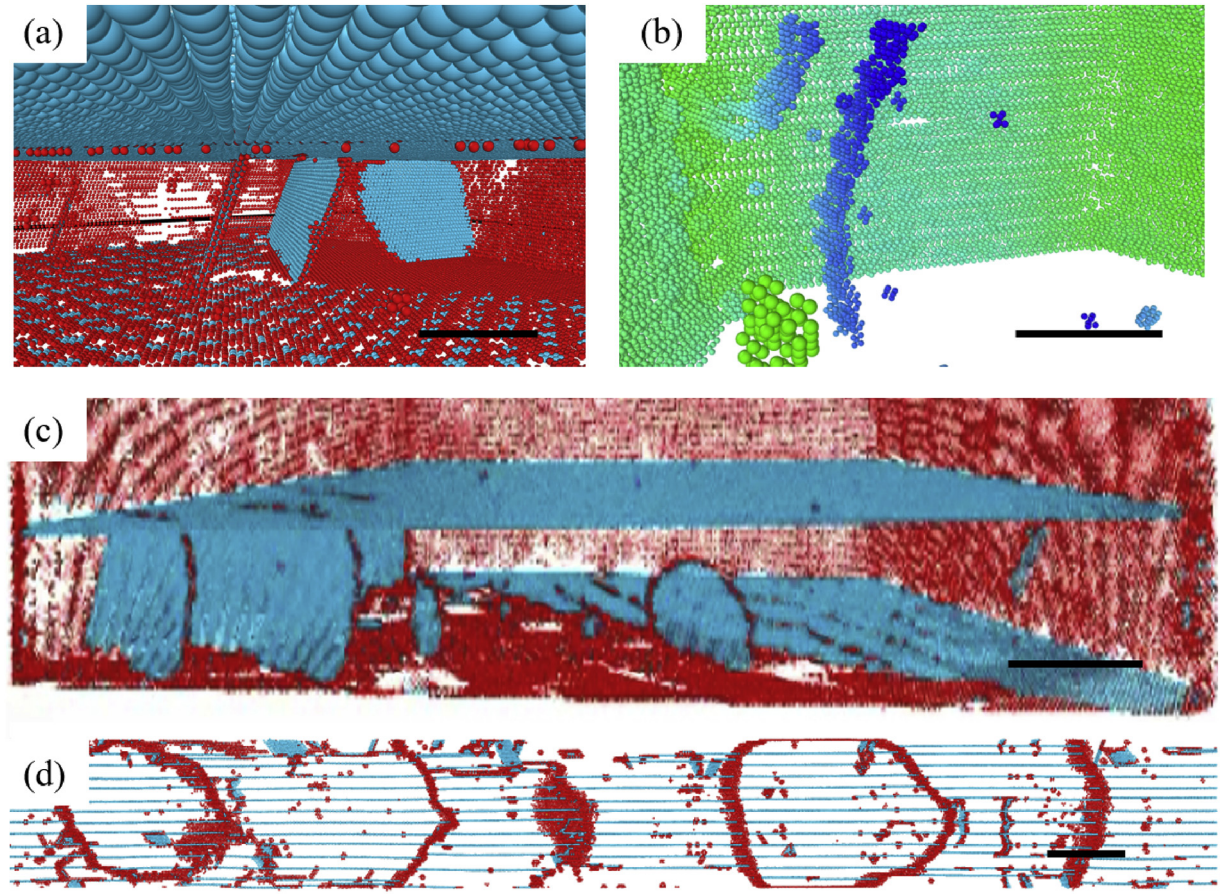

Fig. 11. Deformation patterns of GNT samples with different structural gradients. (a) Threading dislocations governs plastic deformation of NT-B layer with $\lambda_B = 6.3$ nm and $d_B = 50$ nm in all GNT samples. (b) Correlated necklace dislocations (CNDs) governs plastic deformation in NT-A layer with $\lambda_A = 1.04$ nm and $d_A = 50$ nm. (c) A combination of threading dislocations and inclined (Hall-Petch type) dislocations observed in NT-B layer of GNT samples with $g_d = 1$ and $g_\lambda = 5$. (d) Detwinning governed by the glide of twinning partial dislocations at twin boundaries in GNT samples with $g_d = 3$ and $g_\lambda = 5$. Colors are assigned to atoms according to their local lattice structure in (a, c, d) and spatial coordinates in (b). The scale bar stands for a length of 5 nm.

dominant at twin thicknesses above 5 nm [19,48]. This may explain the slight increase in yield strength of the GNT samples when the gradient in twin thickness, g_λ, increases from 0 to 1. Since λ multiplies its logarithm in Eq. (13), the CLS model would predict a stress drop when the twin thickness approaches 1 nm [19], and thus fail to fully capture the monotonic increase in yield strength of the GNT samples as g_λ reaches 5 (Fig. 10b).

Fig. 11b shows the deformation pattern at 7.5% strain for the layer NT-A with $d_A = 50$ nm and $\lambda_A = 1.04$ nm, corresponding to a GNT structure with gradient parameters of $g_\lambda = 5$ and $g_d = 0$. It is observed that plastic deformation is governed by necklace-like dislocations extended over multiple twin boundaries, which was referred to as correlated necklace dislocations (CNDs) or jogged dislocations [4,19,49]. Each CND consists of multiple short component dislocations in adjacent nanotwins, connected by either constricted or extended unit jogs at the twin boundaries. The glide of CNDs involves the collective movement of the component dislocations as well as the continuous pinning and depinning of the units jogs at the twin boundaries. The critical stress required for the de-pinning of a CND has been proposed as follows [19]:

$$\sigma_{CND} = M\left(\frac{f_{pin}}{b\lambda} + \tau_0\right) \tag{14}$$

where τ_0 is the lattice friction stress. Here, f_{pin} represents the pinning force exerted by the twin boundaries on the CND during its motion. Our previous simulations have demonstrated that there exists a transition from threading dislocations to CNDs as the twin thickness is reduced below a critical value around 1 nm [19]. Eq. (14) explicitly shows that the critical stress to drive a CND scales with λ^{-1}, leading to a continuous strengthening behavior with increasing g_λ.

As discussed above, the twin gradient effect on strength (Fig. 10b) can be qualitatively captured by either CLS model for moderate g_λ or CND model for large g_λ. To account for the grain gradient effect on strength observed in Fig. 10a, we examined the deformation pattern of the GNT sample with $g_d = 1$ and $g_\lambda = 5$. Fig. 11c shows the deformation pattern at 7.5% strain for the layer NT-B. We observed the nucleation of threading dislocations from the lateral grain boundaries, which is similar to those found in Fig. 11a. In addition, we observed dislocation loops emitting from the interface between the two layers NT-A and NT-B and gliding toward nearby twin boundaries. These are frequently referred to as mode I dislocations in the literature [45,50,51]. The activation of a particular dislocation type depends on the local stress state. According to the Schmid factor calculations of dislocations in highly oriented nanotwinned structures [45], mode I dislocations are supposed to dominate plastic deformation when the external loading is perpendicular to the twin boundaries, while mode II dislocations are dominant when loading is parallel to the twin boundaries. The simultaneous activation of mode I and mode II dislocations is thus unexpected and must be related to the change of local stress state induced by the substantial structural gradient [2,4,51–53]. Different from the Burgers vectors of threading dislocations that are parallel to the twin boundaries, the Burgers vectors of mode I dislocation are inclined to the twin boundaries. Since twin boundaries provide adequate barriers to the slip of these inclined mode I dislocations, the dependence of yield strength on twin thickness can be written in the form of the classical Hall-Petch (HP) strengthening law, $\sigma_{HP} \propto \lambda^{-1/2}$ [48,54]. It is known that flow stress controlled by HP strengthening is much higher than that controlled by CLS strengthening [48]. More importantly, it has been revealed that the simultaneous activation of mode I and mode II dislocations can trigger the formation of bundles of concentrated dislocations uniformly distributed in grain interiors, leading to a unique patterning of geometrically necessary dislocation with ultra-high dislocation densities [4]. This is believed to cause the extra strengthening observed for GNT samples with $g_d = 1$ (Fig. 10a).

It is intriguing to observe the maximum strength around a critical grain gradient $g_d = 1$. We will next investigate the physical origin of the stress drop above this critical gradient. Fig. 11d shows the deformation pattern at 15% strain for the layer NT-A with $d_A = 12.5$ nm and $\lambda_A = 1.04$ nm, corresponding to a GNT structure with gradient parameters of $g_\lambda = 5$ and $g_d = 3$. Twinning partial dislocations are observed to glide along numerous twin planes, leading to the migration of twin boundaries and the coarsening of the twin lamellae. It is seen that detwinning occurs primarily at the interface between the layers NT-A and NT-B where local stress state is changed by the substantial structural gradient and resolved shear stress is sufficiently high to drive the movement of twinning partial dislocations along the twin boundaries. The nucleation of the twinning partial dislocations should be assisted by the stress concentration at the grain boundaries or the misfit segments at the interface left by the threading dislocations in the layer NT-B. Apparently, the number of nucleation sources of the twinning partial dislocations at the interface increases with increasing grain gradient, i.e., $n_s \propto g_d$. Following the approach developed by Li et al. [55], we derive the critical stress required to activate nucleation-governed detwinning at the interface as follows:

$$\sigma_d = \sigma_a - kln\left(\alpha(g_d + 1)\frac{d_B}{\lambda_A}\right) \tag{15}$$

where σ_a stands for the athermal resistance to dislocation nucleation. The pre-factor k of the second term on the right-hand side of Eq. (15) depends on temperature, local stress concentration and activation volume. The pre-factor in the logarithm, α, is related to Debye frequency and strain rate. For a given d_B and λ_A, it could be seen that the flow stress decreases with increasing grain gradient g_d, consistent with our current simulations results (Fig. 10a). Eq. (15) also suggests that the yield strength decreases with decreasing twin thickness, which has been known as the nucleation-governed softening behavior of nanotwinned metals when the twin thickness drops below a critical value [55]. The dependence of flow stress on twin thickness is thus determined by the competition between CND-governed strengthening (Eq. (14)) and detwinning-governed softening (Eq. (15)). Since the twin thickness is in the logarithmic function in Eq. (15), the magnitude of detwinning-induced stress reduction ($\propto \ln\lambda$) is weaker than that that of CND-induced stress enhancement ($\propto \lambda^{-1}$) as λ decreases. As a result, for a given g_d, the flow stress should increase with increasing g_λ as indicated in Fig. 10b.

The effect of grain/twin gradients on strength and deformation mechanisms of GNT Cu has been summarized in Table 4 for comparison. In the regime of threading dislocations, the confined layer slip (CLS) model (Eq. (13)) can be used to account for the strengthening of GNT samples for moderate g_λ. In the regime of CNDs, the jog-depinning model (Eq. (14)) is essential to capture the continuous strengthening behavior of GNT samples for large g_λ, as the CLS model fails when the twin thickness is comparable to the cutoff radius of dislocation cores. As g_d increases, the classical Hall-Petch (HP) model based on the mechanism of dislocation slip inclined to twin boundaries should be incorporated to explain the extra strengthening of GNT samples. However, the reduced grain size also promotes the nucleation of twinning partial dislocations at

Table 4
Gradient effect on strength and deformation mechanism of GNT Cu.

Structural gradient	Deformation mechanism	Strength
Twin gradient, g_λ	Threading dislocations	Strengthening
	Correlated necklace dislocations	Strengthening
Grain gradient, g_d	Inclined slip to twin boundaries	Strengthening
	Twinning partial dislocations	Softening

the interface, leading to a detwinning-induced softening mechanism (Eq. (15)) for large g_d. The competition between HP strengthening and detwinning-induced softening leads to a maximum strength at a critical g_d.

5. Conclusions

This paper presents a material system design space exploration framework that integrates atomistic simulations, Gaussian process (GP) based active learning surrogate modeling, and optimization for material design and innovation. In the developed framework, the GP-based surrogate model employing the expected improvement based sequential sampling (EISS) technique exhibits the capability of modeling a highly nonlinear feature-property relationship with a high model fidelity using a limited number of selected sampling points. The trade-off between the fidelity of surrogate model and the expense of generating new sample points can be balanced by employing the EISS based sampling technique to adaptive identify the critical sampling points for enhancing the fidelity of the surrogate model in an iterative manner. Employing adaptive sampling and surrogate modeling, we address the challenges of efficiently exploring the material design space while the computationally expensive physics-based simulation is used in material design and discovery.

The developed effective material design space exploration technique has been applied to study the effects of structural gradients on the strength of CNT Cu and identify the optimal design with target material properties. Combining physics-based MD simulation and active learning based surrogate modeling, valuable insights can be obtained efficiently about the relationship between the structural gradients and the strength of CNT Cu. The present study undercovers the collective effects of grain/twin gradients on strength and deformation mechanisms, and demonstrates the importance of creating sufficiently large twin gradients in GNT samples, as the strength is found to increase with increasing twin gradient regardless of the grain gradient involved in the GNT structure. More importantly, the presented findings point out that it is crucial to carefully design the grain gradient of GNT samples because there exists a critical grain gradient at which the strength is maximized. Above the critical grain gradient, a detwinning-induced softening mechanism would become dominant and the strength will decrease with further increasing grain gradient.

In this paper, two design parameters, the grain gradient and the nanotwin gradient, are considered through replicates with random initial samples in a single objective optimization problem, which enables the usage of gradient optimization to identify the optimal design in the current study. In the future work, the developed material design space exploration technique with active learning based surrogate modeling can be extended to considering multiple different material performances such as strength, ductility as well as fatigue resistance, and accordingly multidisciplinary optimization problem could be formulated and advanced global optimization techniques can be adopted in seeking optimum material system designs.

CRediT authorship contribution statement

Xin Chen: Methodology, Software, Validation, Writing - review & editing. **Haofei Zhou:** Conceptualization, Methodology, Writing - original draft, Writing - review & editing, Project administration. **Yumeng Li:** Conceptualization, Methodology, Writing - original draft, Writing - review & editing, Project administration, Funding acquisition.

Acknowledgments

H. Zhou acknowledges support by Zhejiang University through "Hundred Talents Program" and NSFC (No. 11902289). X. Chen and Y. Li are grateful for the support provided by the University of Illinois at Urbana-Champaign. The authors are grateful to Prof. H.J. Gao for insightful discussions.

References

[1] T.H. Fang, et al., Revealing extraordinary intrinsic tensile plasticity in gradient nano-grained copper, Science 331 (6024) (2011) 1587–1590.
[2] X.L. Wu, et al., Extraordinary strain hardening by gradient structure, Proc. Natl. Acad. Sci. U. S. A. 111 (20) (2014) 7197–7201.
[3] Y.J. Wei, et al., Evading the strength- ductility trade-off dilemma in steel through gradient hierarchical nanotwins, Nat. Commun. 5 (2014).
[4] Z. Cheng, et al., Extra strengthening and work hardening in gradient nanotwinned metals, Science 362 (6414) (2018) 559 (-+).
[5] T. Roland, et al., Fatigue life improvement through surface nanostructuring of stainless steel by means of surface mechanical attrition treatment, Scr. Mater. 54 (11) (2006) 1949–1954.
[6] K. Lu, Making strong nanomaterials ductile with gradients, Science 345 (6203) (2014) 1455–1456.
[7] K. Lu, J. Lu, Nanostructured surface layer on metallic materials induced by surface mechanical attrition treatment, Mater. Sci. Eng. A 375 (2004) 38–45.
[8] X.L. Wu, et al., Synergetic strengthening by gradient structure, Mater. Res. Lett. 2 (4) (2014) 185–191.
[9] Y. Liu, Y.J. Wei, Gradient driven anomalous reversible plasticity in conventional magnesium alloys, Extreme Mech. Lett. 9 (2016) 158–164.
[10] Y. Lin, et al., Mechanical properties and optimal grain size distribution profile of gradient grained nickel, Acta Mater. 153 (2018) 279–289.
[11] Y. Li, G.D. Seidel, Multiscale modeling of the effects of nanoscale load transfer on the effective elastic properties of unfunctionalized carbon nanotube-polyethylene nanocomposites, Model. Simul. Mater. Sci. Eng. 22 (2) (2014).
[12] Y. Li, G.D. Seidel, Multiscale modeling of functionalized interface effects on the effective elastic material properties of CNT-polyethylene nanocomposites, Comput. Mater. Sci. 107 (2015) 216–234.
[13] Y. Li, G.D. Seidel, Multiscale modeling of the interface effects in CNT-epoxy nanocomposites, Comput. Mater. Sci. 153 (2018) 363–381.
[14] A.H. Esbati, S. Irani, Effect of functionalized process and CNTs aggregation on fracture mechanism and mechanical properties of polymer nanocomposite, Mech. Mater. 118 (2018) 106–119.
[15] Y.P. Yan, Y.X. Lei, S. Liu, Tensile responses of carbon nanotubes-reinforced copper nanocomposites: molecular dynamics simulation, Comput. Mater. Sci. 151 (2018) 273–277.
[16] B.D. Jensen, et al., Simulating the effects of carbon nanotube continuity and interfacial bonding on composite strength and stiffness, Compos. Sci. Technol. 166 (2018) 10–19.
[17] W.B. Li, F.P. Yuan, X.L. Wu, Atomistic tensile deformation mechanisms of Fe with gradient nano-grained structure, AIP Adv. 5 (8) (2015).
[18] K. Zhou, et al., Molecular dynamics simulations of tensile deformation of gradient nano-grained copper film, Comput. Mater. Sci. 142 (2018) 389–394.
[19] H.F. Zhou, et al., A jogged dislocation governed strengthening mechanism in nanotwinned metals, Nano Lett. 14 (9) (2014) 5075–5080.
[20] Z.Q. Wang, P.F. Wang, A double-loop adaptive sampling approach for sensitivity-free dynamic reliability analysis, Reliab. Eng. Syst. Saf. 142 (2015) 346–356.
[21] P.F. Wang, Z.Q. Wang, A.T. Almaktoom, Dynamic reliability-based robust design optimization with time-variant probabilistic constraints, Eng. Optim. 46 (6) (2014) 784–809.
[22] Z.Q. Wang, P.F. Wang, A maximum confidence enhancement based sequential sampling scheme for simulation-based design, J. Mech. Des. 136 (2) (2014).
[23] Z. Wang, P. Wang, A nested extreme response surface approach for time-dependent reliability-based design optimization, J. Mech. Des. 134 (12) (2012) 121007–121007-14.
[24] D.R. Jones, M. Schonlau2, W.J. Welch, Efficient global optimization of expensive black-box functions, J. Glob. Optim. 13 (4) (1998) 37.
[25] M. Stein, Large sample properties of simulations using Latin hypercube sampling, Technometrics 29 (2) (1987) 143–151.
[26] T. Goel, R.T. Haftka, W. Shyy, Error measures for noise-free surrogate approximations, in: AIAA Paper, 2008, pp. 2008–2901.
[27] A. Dey, S. Mahadevan, Ductile structural system reliability analysis using adaptive importance sampling, Struct. Saf. 20 (2) (1998) 137–154.
[28] L. Martino, et al., An adaptive population importance sampler: learning from uncertainty, IEEE Trans. Signal Process. 63 (16) (2015) 4422–4437.
[29] B. Beachkofski, R. Grandhi, Improved distributed hypercube sampling, in: 43rd AIAA/ASME/ASCE/AHS/ASC Structures, Structural Dynamics, and Materials Conference, 2002. April.
[30] S. Leary, A. Bhaskar, A. Keane, Optimal orthogonal-array-based latin hypercubes, J. Appl. Stat. 30 (5) (2003) 585–598.
[31] V.R. Joseph, Y. Hung, Orthogonal-maximin Latin hypercube designs, Stat. Sin. 18 (1) (2008) 171–186.
[32] J.L. Deutsch, C.V. Deutsch, Latin hypercube sampling with multidimensional uniformity, J. Stat. Plan. Infer. 142 (3) (2012) 763–772.
[33] A. Mannodi-Kanakkithodi, et al., Machine learning strategy for accelerated design of polymer dielectrics, Sci. Rep. 6 (2016).
[34] L. Bassman, et al., Active learning for accelerated design of layered materials,

npj Comput. Mater. (4) (2018).
[35] N. Artrith, A. Urban, An implementation of artificial neural-network potentials for atomistic materials simulations: performance for TiO2, Comput. Mater. Sci. 114 (2016) 135–150.
[36] Y. Li, W. Xiao, P. Wang, Uncertainty quantification of artificial neural network based machine learning potentials, in: ASME 2018 International Mechanical Engineering Congress and Exposition, ASME, Pittsburgh, 2018.
[37] Y. Li, P. Wang, W. Xiao, Uncertainty quantification of atomistic materials simulation with machine learning potentials, in: AIAA Non-Deterministic Approaches Conference, 2018, American Institute of Aeronautics and Astronautics Inc, AIAA, Kissimmee, 2018.
[38] R.Y. Rubinstein, D.P. Kroese, Simulation and the Monte Carlo Method second ed., vol. 707, John Wiley & Sons, 2011.
[39] L. Lu, et al., Revealing the maximum strength in nanotwinned copper, Science 323 (5914) (2009) 607–610.
[40] W.G. Hoover, Constant-pressure equations of motion, Phys. Rev. A 34 (3) (1986) 2499–2500.
[41] S. Nose, A unified formulation of the constant temperature molecular-dynamics methods, J. Chem. Phys. 81 (1) (1984) 511–519.
[42] Y. Mishin, et al., Structural stability and lattice defects in copper: ab initio, tight-binding, and embedded-atom calculations, Phys. Rev. B 63 (22) (2001).
[43] J.D. Honeycutt, H.C. Andersen, Molecular-dynamics study of melting and freezing of small Lennard-Jones clusters, J. Phys. Chem. 91 (19) (1987) 4950–4963.
[44] H. Liu, Y.-S. Ong, J. Cai, A survey of adaptive sampling for global metamodeling in support of simulation-based complex engineering design, Struct. Multidiscip. Optim. 57 (1) (2018) 393–416.
[45] Q.H. Lu, et al., Dependence of dislocation structure on orientation and slip systems in highly oriented nanotwinned cu, Acta Mater. 127 (2017) 85–97.
[46] W.D. Nix, Yielding and strain hardening of thin metal films on substrates, Scr. Mater. 39 (4–5) (1998) 545–554.
[47] A. Misra, J.P. Hirth, R.G. Hoagland, Length-scale-dependent deformation mechanisms in incoherent metallic multilayered composites, Acta Mater. 53 (18) (2005) 4817–4824.
[48] Z.S. You, et al., Plastic anisotropy and associated deformation mechanisms in nanotwinned metals, Acta Mater. 61 (1) (2013) 217–227.
[49] H.F. Zhou, H.J. Gao, A plastic deformation mechanism by necklace dislocations near crack-like defects in Nanotwinned metals, J. Appl. Mech. 82 (7) (2015).
[50] K. Lu, Stabilizing nanostructures in metals using grain and twin boundary architectures, Nat. Rev. Mater. 1 (5) (2016).
[51] M.X. Yang, et al., Back stress strengthening and strain hardening in gradient structure, Mater. Res. Lett. 4 (3) (2016) 145–151.
[52] Z. Zeng, et al., Gradient plasticity in gradient nano-grained metals, Extreme Mech. Lett. 8 (2016) 213–219.
[53] Y. Wang, et al., Optimal stress and deformation partition in gradient materials for better strength and tensile ductility: a numerical investigation, Sci. Rep. 7 (2017).
[54] K. Lu, L. Lu, S. Suresh, Strengthening materials by engineering coherent internal boundaries at the nanoscale, Science 324 (5925) (2009) 349–352.
[55] X.Y. Li, et al., Dislocation nucleation governed softening and maximum strength in nano-twinned metals, Nature 464 (7290) (2010) 877–880.